Chemical Science

EDGE ARTICLE

View Article Online
View Journal | View Issue

Cite this: *Chem. Sci.*, 2018, **9**, 6150

All publication charges for this article have been paid for by the Royal Society of Chemistry

Organic emitter integrating aggregation-induced delayed fluorescence and room-temperature phosphorescence characteristics, and its application in time-resolved luminescence imaging†

Fan Ni,‡[ab] Zece Zhu,‡[a] Xiao Tong,[c] Mingjuan Xie,[c] Qiang Zhao,*[c] Cheng Zhong,[a] Yang Zou[b] and Chuluo Yang*[ab]

Received 1st April 2018
Accepted 28th June 2018

DOI: 10.1039/c8sc01485j

rsc.li/chemical-science

Thermally activated delayed fluorescence (TADF) with a substantially long lifetime furnishes a new paradigm in developing probes for time-resolved imaging. Herein, a novel TADF fluorophore, namely, **PXZT**, with terpyridine as the acceptor and phenoxazine (PXZ) as the donor, was rationally designed and synthesized. The new compound shows typical thermally activated delayed fluorescence, aggregation-induced emission and crystallization-induced room-temperature phosphorescence (RTP). The coordination of **PXZT** with a zinc ion causes the quenching of the fluorescence of **PXZT** due to the enhanced intramolecular charge transfer of the resulting complex **ZnPXZT1**. With the dissociation of the **ZnPXZT1** to release **PXZT** and the subsequent *in situ* hydrophobic aggregation of the free **PXZT** to resist the influence of oxygen, the TADF emission of **PXZT** is recovered. This zinc-assisted process is successfully used for time-resolved imaging of HeLa and 3T3 cells. This work presents a simple and effective strategy for time-resolved imaging by *in situ* forming TADF aggregates to turn on the TADF emission.

Introduction

Time-resolved luminescence imaging (TRLI) has revolutionized contemporary visualization methods by facilitating indispensable advancements in the observation of functional and molecular recognition events in the cell.[1] By setting a suitable delay time between the pulsed excitation light and the long-lived luminescence of the exploited luminophore, TRLI presents an elegant solution to the problem of short-lived background signals scattering or vanishing from the observed medium. Consequently, it has made the acquisition of a high signal-to-noise ratio possible during imaging measurements.[2]

In general, to pursue the attractive advantages in TRLI, a basic parameter that should be possessed by the employed luminophore is a relatively long excited-state lifetime. In the past few decades, interest in luminophores with a long-lived triplet state has emerged and witnessed tremendous progress in association with TRLI. Due to the suitable long lifetimes (from microseconds to milliseconds), phosphorescence transition-metal (*e.g.*, Ru(II),[3] Ir(III),[4] Pt(II),[5] and Ln(III)[6]) complexes have been verified to play a key role in TRLI. In addition, pure organic luminophores that feature long-lived room-temperature phosphorescence (RTP)[7] have also been incorporated in TRLI. As a result of their pertinent features, phosphorescence-based luminophores have demonstrated appealing prospects and presented practical channels for designing probes for TRLI.

Very recently, a great breakthrough has been made in the field of long-lived singlet-state emissive luminophores.[8] Pure organic thermally activated delayed fluorescence (TADF) materials accompanied by effective singlet-state emission and appropriately long lifetimes can theoretically offer advantages for time-resolved imaging. Aside from the essential long emission lifetimes, the structural diversity and emissive adjustability also make TADF-based luminophores ideal alternatives for use within organisms. However, the design of TADF-based probes for biological imaging, especially for TRLI, remains a big

[a]*Department of Chemistry, Hubei Key Lab on Organic and Polymeric Optoelectronic Materials, Wuhan University, Wuhan, 430072, P. R. China. E-mail: clyang@whu.edu.cn*

[b]*Shenzhen Key Laboratory of Polymer Science and Technology, College of Materials Science and Engineering, Shenzhen University, Shenzhen, 518060, P. R. China*

[c]*Key Laboratory for Organic Electronics & Information Displays, Institute of Advanced Materials, Nanjing University of Posts and Telecommunications, Nanjing, 210023, P. R. China. E-mail: iamqzhao@njupt.edu.cn*

† Electronic supplementary information (ESI) available: Synthesis and additional figures details. CCDC 1497984–1497986. For ESI and crystallographic data in CIF or other electronic format see DOI: 10.1039/c8sc01485j

‡ These authors contributed equally to this work.

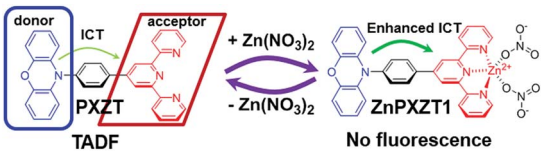

Scheme 1 Proposed mechanism for zinc ion-assisted regulation of thermally activated delayed fluorescence.

challenge.[9] The sensitivity of the excited triplet state in TADF emitters to oxygen is the most significant obstacle for their application. In 2014, by employing BSA to eliminate singlet oxygen and enhance the intensity of delayed fluorescence, Peng *et al.* revealed a TADF-based time-resolved platform to achieve fluorescence sensing in MCF-7 cancer cells, which proves the feasibility of TADF emitters for TRLI.[9a] In 2016, as a means to eliminate the influence of oxygen, Huang *et al.* proposed an efficient strategy of embedding aggregates of TADF dyes into a diblock polymer matrix.[9d] The creative approach opened up a new opportunity for TRLI in living cells. Despite the progress, developing reaction-based probes to turn on the delayed fluorescence while achieving the specific detection has become a burning issue.

To solve the problem of the triplet state quenching of TADF-based probes in an oxygen-containing atmosphere,[10] herein, we reported a new strategy by *in situ* aggregation-induced TADF turn-on response. This is unlike the previously reported approach of excluding oxygen with additional assistance or preparing aggregates before the detection to cut off oxygen access.

First, the luminophore **PXZT** was constructed based on a practical D–A-type structure with phenoxazine (**PXZ**) and terpyridine as the donor and acceptor units, respectively. The luminophore **PXZT** demonstrated ideal emission properties and typical TADF features. Next, the coordination of the luminophore **PXZT** with a zinc ion to form **ZnPXZT1** was conducted. The coordination process greatly enhanced the intramolecular charge transfer (ICT), and thus quenched the self-fluorescent emission of **PXZT**, which can reduce the background signal. Finally, the water-soluble complex of **ZnPXZT1** was successfully employed in time-resolved imaging of HeLa and 3T3 cells by ingeniously releasing TADF emitter of **PXZT** *via* the *in situ* dissociation of **ZnPXZT1** in cell. The monitored long-lived emission of **PXZT** during the TRLI in live cells suggested **ZnPXZT1** is a practical probe for cellar imaging (Scheme 1).

Results and discussion

1 TADF features of PXZT

Serving as a D–A-type molecule, **PXZT** shows obvious intramolecular charge transfer (ICT) characteristics. The strong absorption bands at approximately 275 and 315 nm can be attributed to the π–π* electronic transition, while the broad absorption band from 360 nm to 450 nm can be ascribed to the ICT transition from the **PXZ** unit to the terpyridine unit (Fig. S3†). The emission spectra of **PXZT** displayed the

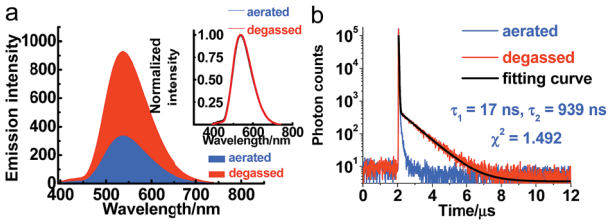

Fig. 1 Steady-state emission spectra (a) and transient photoluminescence decay spectra (b) of PXZT in 2-methyltetrahydrofuran at room temperature with and without degassing with argon, λ_{ex} = 377 nm, λ_{em} = 540 nm.

significant red shift with the increasing solvent polarity (Fig. S4†), demonstrating positive solvatochromism. Due to the strong charge transfer effect, employing highly polar DMSO or ethanol as the solvent led to quenching of the emission.[8e,f] These results provided a paradigm for the design of a turn-on-type probe with regulation of the ICT intensity in **PXZT**.

The emission spectra of **PXZT** in toluene under degassed and aerated conditions were measured to evaluate the sensitivity of **PXZT** emission to oxygen. The fluorescence intensities of the **PXZT** solutions (in toluene and 2-methyltetrahydrofuran) after degassing with argon were stronger than those under aerated conditions (Fig. 1a and S5a†). The transient photoluminescence decay spectra of **PXZT** in solution after degassing with argon showed biexponential fluorescence decays (Fig. 1b and S5b†). When exposed to air, the dilute solution only showed a short-lived emission. The obvious quenching of the emission of the **PXZT** solution by oxygen implied that the luminophore **PXZT** can hardly be used for TRLI in oxygen-containing environment.

A time-gated measurement of the emission of **PXZT** in a 2-methyltetrahydrofuran solution at room temperature after degassing with argon was conducted to determine the origins of the prompt and delayed emissions. The normalized spectrum with a delay time of 595 ns overlapped well with the spectrum with a delay time of 10 ns (Fig. S6†), which directly demonstrated that the emission of **PXZT** resulted from its radiative relaxation from the excited singlet state.

The transient emission of **PXZT** in 2-methyltetrahydrofuran at different temperatures after degassing was carefully measured. With the rising temperature, the steady-state emission intensity and the ratios of the delayed components of the **PXZT** emission increased obviously (Fig. 2a and b), proving that

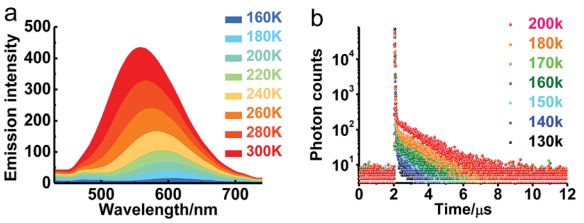

Fig. 2 Steady-state emission spectra (a) and transient photoluminescence decay spectra (b) of PXZT in 2-methyltetrahydrofuran at different temperatures after degassing with argon, λ_{ex} = 377 nm, λ_{em} = 540 nm.

thermal energy accelerates the process of reverse intersystem crossing.

With **PXZT** in degassed toluene and 2-methyltetrahydrofuran solutions owing TADF features, the emissive characteristics of **PXZT** in solid state were also recorded. Even in air, the doped PMMA film containing 5 wt% **PXZT** showed a long-lived emission in the microsecond range (Fig. S7†). This result implied that dense packing in solid state may restrain the quench of air to the triplet state of **PXZT**, which can be utilized for TRLI in oxygen-containing atmosphere. The delay lifetime and emission intensity of **PXZT** in the PMMA film were reasonably longer in an argon atmosphere than those in air. In the time-gated measurements, the normalized spectrum at a delaytime of 0.1 ms overlapped well with the steady-state spectrum (Fig. S8†). This indicated that the delayed emission in the doped PMMA film also resulted from the radiative relaxation from the exited singlet state.

As the aggregation of **PXZT** can also form dense packing, the steady-state emission spectra and transient photoluminescence decay spectra of **PXZT** in THF/water mixtures with different volume ratios were investigated in air. The steady-state emission in air demonstrated typical twisted intramolecular charge transfer (TICT) at a low proportion of water and aggregation-induced emission enhancement behavior with the continuously increasing the proportion of water (f_w) (Fig. 3a and b). With the increase of f_w or the concentration of **PXZT**, the lifetimes of the prompt fluorescence showed no obvious change, while the lifetimes and ratios of the delayed components obviously increased, demonstrating aggregation-induced TADF emission enhancement (Fig. 3c and d, Tables S1 and S2†). These positive results presented a practical channel for turning on the TADF of **PXZT** by its *in situ* aggregation for TRLI in oxygen-containing environment.

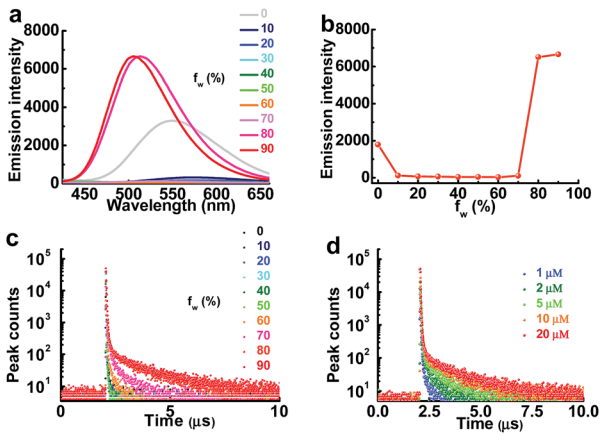

Fig. 3 (a) Steady-state emission spectra of 20 μM **PXZT** in THF and water mixtures at different f_w in air, λ_{ex} = 340 nm. (b) The emission intensity at 506 nm with the change of f_w, λ_{ex} = 340 nm. (c) Transient photoluminescence decay spectra of **PXZT** in THF/water mixtures with different f_w in air, λ_{ex} = 377 nm. (d) Transient photoluminescence decay spectra of different concentration of **PXZT** in THF/water mixtures (f_w = 90) in air, λ_{ex} = 377 nm, λ_{em} = 506 nm.

2 Luminescent properties of the PXZT in regularly arranged solid state

To further understand the photophysical properties of solid **PXZT** in the regular packing state, the emission of a single crystal of **PXZT** was measured. Unlike the emission in solutions or film doped in PMMA, a much longer emission lifetime in the millisecond range was observed. In time-gated measurements with a delay time of 0.5 ms, **PXZT** showed an emission peak at approximately 560 nm, which presented a remarkable redshift of approximately 100 nm with respect to its steady state spectrum (Fig. 4a). The emission lifetime at room temperature was approximately 11 ms (Fig. S11†), which is much longer than that in solution or in doped PMMA film. Based on above observations, the crystallization-induced room temperature phosphorescence of **PXZT** may be a possible avenue for exploration.

To confirm the mechanism of the phosphorescence emission, the transient photoluminescence decay spectra of crystalline **PXZT** were measured at different temperatures. With the decreasing temperature, the emission decay became slower (Fig. 4b). At 77 K, the lifetime at 560 nm was 0.4 s (Fig. S11†). The stable T_1 state at 77 K radiated more slowly and phosphoresced over a longer lifetime.

The single-crystal analysis of **PXZT** revealed the face-to-face antiparallel packing mode between the two planes of adjacent **PXZT** molecules (Fig. S12a†). The obvious π–π stacking (3.42 Å) between the moiety of the electron-poor terpyridine in the two stacking molecules occurred in the opposite direction. The electron-rich **PXZ** in two neighbouring molecules also stacked with each other (3.59 Å) (Fig. S12b†). C–H···O (2.59 Å) and C–H···N (2.74 Å) hydrogen bonds existed in the crystal structure can further stabilize the crystal structure (Fig. S12c†). Similar to the conditions observed in many organic crystals,[7b,c] the intermolecular interaction in **PXZT** can stabilize the triplet state and decrease its decay rate with the room-temperature luminescence lasting for tens of milliseconds.

To identify the role of π–π stacking in the crystal state and to explain the above phenomena, natural transition orbital (NTO) calculations were carried out. The calculated NTO pairs for the first excited singlet state were localized on a phenoxazine and a terpyridine unit, while the NTO pairs of the first triplet excited

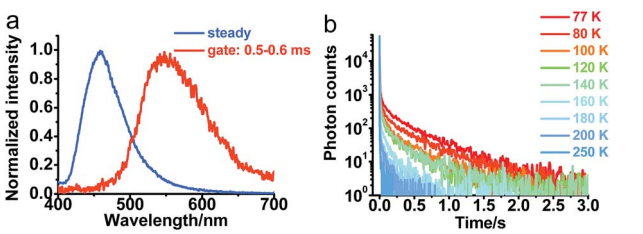

Fig. 4 (a) Normalized steady-state and time-gated emission spectra of the crystal of **PXZT** at room temperature in air. The energy of first excited singlet state E_S = 3.00 eV, the energy of first excited triplet state E_T = 2.55 eV, and the singlet-triplet splitting energy ΔE_{ST} = 0.45 eV. (b) Transient photoluminescence decay spectra of the crystal of **PXZT** at different temperatures under Ar, λ_{ex} = 377 nm, λ_{em} = 560 nm.

state were localized on the aggregated terpyridine units (Fig. S13b†). According to the calculations, the first excited singlet state of the crystal was a charge-transfer state, while the first triplet state was a localized electronic state. The localized electronic state delocalized significantly as terpyridine formed π–π stacking in the crystalline state, which may decrease the triplet state energy.

Then the fluorescence and phosphorescence emission in PMMA film and crystalline state were compared to understand the reason why the TADF was switched to RTP in regularly arranged crystalline state. An obvious blueshift of about 40 nm of the steady-state fluorescence peak in the crystalline state (Fig. S9 and S10†) meant a rise of 0.12 eV of E_S. What's more, a significant redshift of about 55 nm of the phosphorescence peak was observed in the crystalline form relative to that in the PMMA film (Fig. S9 and S10†), and thus E_T was directly reduced by 0.15 eV. Consequently, the ΔE_{ST} in crystalline **PXZT** reached 0.45 eV, which is improper for reverse intersystem crossing (RISC) processing to produce effective TADF emission. And the stabilized triplet state in crystalline state can be account for the room-temperature phosphorescence emission.

3 The TADF quenching of PXZT by zinc ions

Though **PXZT** exhibited long-lived luminescence, its poor solubility in water limited its further application in biological imaging. To achieve a fluorescence and lifetime dual turn-on-type detection, quenching of the TADF emission was imperative. To solve the key issue, a strategy by using the coordination of terpyridine unit of **PXZT** with a zinc ion to enable an enhanced ICT was proposed.[11] Upon the addition of $Zn(NO_3)_2 \cdot 6H_2O$ to a 1,4-dioxane solution of **PXZT**, the fluorescence of the **PXZT** was quenched gradually (Fig. 5). The change in the fluorescence intensity fitted well with a 1 : 1 binding mode,[12] and the dissociation constant (K_d) was estimated to be 9.3 nM.

The formation of **ZnPZXT1** was also monitored by UV titration. The UV titration of **PXZT** upon coordination with a zinc ion in ethanol solution showed the appearance and enhancement of a new charge transfer absorption band with a peak at approximately 430 nm, which was a significant redshift of 55 nm compared to that of **PXZT** (Fig. S14†). Through coordination of **PXZT** with a zinc ion, the fluorescence of **PXZT** was totally quenched, which is benefited to decreasing the background signal in imaging. Moreover, the resulting Zn^{2+} complex also acquired solubility in water. The improved solubility and quenched emission suggested **ZnPXZT1** is an ideal candidate for cell imaging.

4 Time-resolved luminescence cell imaging

The fluorescence recovery of **PXZT** is the key process in time-resolved cell imaging. Since zinc is an essential trace element for eukaryotes[13] and many zinc proteins and participates in a variety of cellular activities,[14] we supposed **ZnPXZT1** may dissociate to free its fluorescent **PXZT** during the cell imaging process.

To investigate the feasibility of fluorescence recovery, **ZnPXZT1** was then utilized for TRLI in cells. After incubating the 10 μM complex for 5 h in HeLa cells, obvious green luminescence signals could be detected (Fig. 6). The luminescence signals were distributed in different regions of the HeLa cells, and the lifetimes of the luminescence signals at different regions were significantly different (Fig. 6d). Considering the lifetimes of cellular autofluorescence were no more than 10 ns,[15] the short-lived fluorescence signals were completely filtrated by a delay time of 50 ns. Due to the luminescence quenching of **ZnPXZT1**, the detected long-lived luminescence signals with lifetimes over 50 ns may come from the long lifetime of delay fluorescence of **PXZT** (Fig. 6e and f), which may be released by the dissociation of **ZnPXZT1** during the cell imaging process.

To further investigate the applicability of the TADF-based technique in other type of cells, the 3T3 cells were incubated with 10 μM complex for **ZnPXZT1**-based TRLI. In the steady-state imaging process, it can be found that obvious green luminescence signals appeared after 5 h incubating (Fig. S16a†). In the luminescence lifetime (Fig. S16d†) and time-gated (Fig. S16e and f†) imaging, the long-lived luminescence signals with lifetimes over 50 ns can also be detected, similar to the case of HeLa cells.

5 Dissociation of ZnPXZT1 *in vitro*

With the successful application of the TADF-based TRLI, the fluorescence titration was carried out to examine our hypothesis

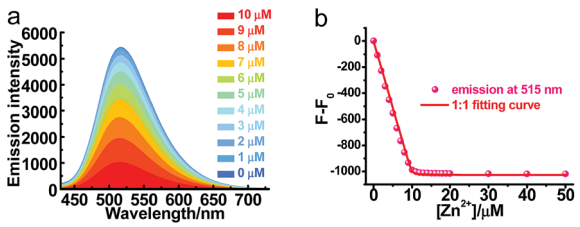

Fig. 5 (a) Steady-state emission spectra of 10 μM PXZT upon the addition of $Zn(NO_3)_2 \cdot 6H_2O$ in dioxane at room temperature, λ_{ex} = 330 nm. (b) The decrease in the emission intensity *vs.* the concentration of zinc ions.

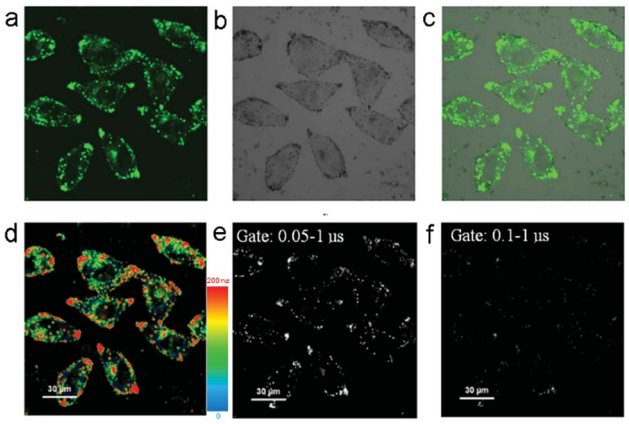

Fig. 6 Steady-state (a–c), luminescence lifetime (d) and time-gated (e and f) imaging of HeLa cells incubated with 10 μM **ZnPXZT1**. λ_{ex} = 405 nm, λ_{em} = 470–570 nm. (a) Darkfield; (b) bright field; (c) merging of (a) and (b).

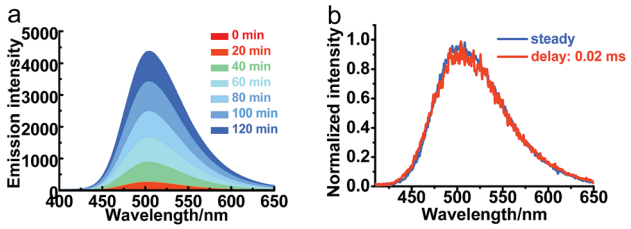

Fig. 7 (a) Steady-state emission spectra of a 20 μM **ZnPXZT1** solution upon the addition of 20 μM EDTA in 10 mM HEPES buffer (pH = 7) at room temperature in air. (b) Normalized steady-state and time-gated emission spectra of a 20 μM **ZnPXZT1** solution upon the addition of 20 μM EDTA in air, λ_{ex} = 330 nm, λ_{em} = 505 nm.

of the dissociation of **ZnPXZT1**. To a solution of 20 μM **ZnPXZT1** in HEPES buffer in air, upon the addition of EDTA (Fig. 7a), the fluorescence intensity of **PXZT** at 505 nm increased significantly with more than 2000-fold of its initial value, which demonstrated an efficient turn-on detection. A long-lived emission with a lifetime in the microsecond range was detected through the transient luminescent spectrum test (Fig. S17†). Based on the time-gated measurement, the normalized spectrum with a delay time of 20 μs overlapped well with the steady-state spectrum, which suggested that the TADF emission of **PXZT** was recovered (Fig. 7b). It is probable that EDTA with strong coordinative ability can effectively bind the zinc ion and remove it from the complex of **ZnPXZT1**, and the ligand of **PXZT** is then released. Subsequently, the *in situ*-generated **PXZT** may aggregate in the buffer due to its insolubility, which inhibits the quenching of **PXZT** fluorescence by oxygen, consequently the TADF emission of **PXZT** was recovered in HEPES buffer in air. To get direct evidence of the dissociation of **ZnPXZT1** in cell, we attempted to do the same test by using several intracellular active species that coordinate with zinc ion with high affinities to replace EDTA, such as cysteine, pyrophosphate, monohydrogen sulfide (Fig. S18†), unfortunately, we failed. This could be due to the complexity of cell environment where some synergistic effect may result in the dissociation of the zinc complex.

Conclusions

In conclusion, a new D–A-type luminophore (**PXZT**) featured with typical TADF and crystallization-induced RTP features was developed. By coordination of **PXZT** with a zinc ion, both the prompt and delayed fluorescence were quenched due to the enhancement of ICT. With the dissociation of **ZnPXZT1** to release **PXZT** and its subsequent hydrophobic aggregation to turn on the aggregation-induced TADF emission, the complex of **ZnPXZT1** was rationally used *in vitro*, which demonstrated an efficient detection of EDTA with more than 2000-fold enhancement of fluorescence intensity. The time-resolved imaging of HeLa and 3T3 cells with **ZnPXZT1** was successfully conducted and found to be an efficient approach to eliminate the background signals. Compared with the previous reported methods of excluding oxygen with additional assistance or prearranged aggregates, the newly proposed strategy with dissociation reaction and aggregation process provides an efficient and practical platform for time-resolved cell imaging by the rational regulation of aggregation-induced TADF emission in oxygen-containing atmosphere (Table S4†). We believe that simple TADF emitters with aggregation-induced delayed fluorescence enhancement will become very promising candidates for time-resolved luminescence imaging.

Conflicts of interest

The authors declare no conflict of interest.

Acknowledgements

We gratefully acknowledge financial support from the Innovative Research Groups of the National Natural Science Foundation (No. 21721005), the National Natural Science Foundation of China (No. 51603152 and 91433201) and the Shenzhen Peacock Plan (KQTD20170330110107046).

Notes and references

1 (*a*) N. Weibel, L. J. Charbonnière, M. Guardigli, A. Roda and R. Ziessel, *J. Am. Chem. Soc.*, 2004, **126**, 4888–4896; (*b*) K. Hanaoka, K. Kikuchi, S. Kobayashi and T. Nagano, *J. Am. Chem. Soc.*, 2007, **129**, 13502–13509; (*c*) D. Jin and J. A. Piper, *Anal. Chem.*, 2011, **83**, 2294–2300; (*d*) L. Gu, D. J. Hall, Z. Qin, E. Anglin, J. Joo, D. J. Mooney, S. B. Howell and M. J. Sailor, *Nat. Commun.*, 2013, **4**, 2326–2332.

2 (*a*) J. C. G. Bünzli and C. Piguet, *Chem. Soc. Rev.*, 2005, **34**, 1048–1077; (*b*) G. Muller, *Dalton Trans.*, 2009, 9692–9707; (*c*) M. Y. Berezin and S. Achilefu, *Chem. Rev.*, 2010, **110**, 2641–2684; (*d*) Z. Zhu, W. Li and C. Yang, *Sens. Actuators, B*, 2016, **224**, 31–36.

3 (*a*) M. R. Gill and J. A. Thomas, *Chem. Soc. Rev.*, 2012, **41**, 3179–3192; (*b*) D. L. Ma, V. P. Y.Ma, D. S. H. Chan, K. H. Leung, H. Z. He and C. H. Leung, *Coord. Chem. Rev.*, 2012, **256**, 3087–3113.

4 (*a*) D. L. Ma, D. S. H. Chan and C. H. Leung, *Acc. Chem. Res.*, 2014, **47**, 3614–3631; (*b*) Y. Yang, Q. Zhao, W. Feng and F. Li, *Chem. Rev.*, 2013, **113**, 192–270; (*c*) H. Shi, H. Sun, H. Yang, S. Liu, G. Jenkins, W. Feng, F. Li, Q. Zhao, B. Liu and W. Huang, *Adv. Funct. Mater.*, 2013, **23**, 3268–3276.

5 T. Zou, J. Liu, C. T. Lum, C. Ma, R. C. Chan, C. N. Lok, W. M. Kwok and C. M. Che, *Angew. Chem., Int. Ed.*, 2014, **126**, 10283–10287.

6 (*a*) E. A. Weitz, J. Y. Chang, A. H. Rosenfield and V. C. Pierre, *J. Am. Chem. Soc.*, 2012, **134**, 16099–16102; (*b*) M. Delbianco, V. Sadovnikova, E. Bourrier, G. Mathis, L. Lamarque, J. M. Zwier and D. Parker, *Angew. Chem., Int. Ed.*, 2014, **53**, 10718–10722; (*c*) Z. Dai, L. Tian, B. Song, Z. Ye, X. Liu and J. Yuan, *Anal. Chem.*, 2014, **86**, 11883–11889; (*d*) Z. Zhu, B. Song, J. Yuan and C. Yang, *Adv. Sci.*, 2016, **3**, 1600146.

7 (*a*) M. Palner, K. Pu, S. Shao and J. Rao, *Angew. Chem., Int. Ed.*, 2015, **54**, 11477–11480; (*b*) X. Zhen, Y. Tao, Z. An,

P. Chen, C. Xu, R. Chen, W. Huang and K. Pu, *Adv. Mater.*, 2017, **29**, 1606665; (*c*) W. Z. Yuan, X. Y. Shen, H. Zhao, J. W. Y. Lam, L. Tang, P. Lu, C. Wang, Y. Liu, Z. Wang, Q. Zheng, *et al.*, *J. Phys. Chem. C*, 2010, **114**, 6090–6099; (*d*) O. Bolton, K. Lee, H. J. Kim, K. Y. Lin and J. Kim, *Nat. Chem.*, 2011, **3**, 205–210; (*e*) Q. Miao, C. Xie, X. Zhen, Y. Lyu, H. Duan, X. Liu, J. Jokerst and K. Pu, *Nat. Biotechnol.*, 2017, **35**, 1102–1110.

8 (*a*) M. Y. Wong and E. Zysman-Colman, *Adv. Mater.*, 2017, **29**, 1605444; (*b*) Z. Yang, Z. Mao, Z. Xie, Y. Zhang, S. Liu, J. Zhao, J. Xu, Z. Chi and M. P. Aldred, *Chem. Soc. Rev.*, 2017, **46**, 915–1016; (*c*) Y. Im, M. Kim, Y. J. Cho, J. A. Seo, K. S. Yook and J. Y. Lee, *Chem. Mater.*, 2017, **29**, 1946–1963; (*d*) Z. Zhu, D. Tian and X. Shu, *Sens. Actuators, B*, 2018, **260**, 289–294; (*e*) R. Ishimatsu, S. Matsunami, K. Shizu, C. Adachi, K. Nakano and T. Imato, *J. Phys. Chem. A*, 2013, **117**, 5607–5612; (*f*) T. J. Penfold, F. B. Diasb and A. P. Monkman, *Chem. Commun.*, 2018, **54**, 3926–3935.

9 (*a*) X. Xiong, F. Song, J. Wang, Y. Zhang, Y. Xue, L. Sun, N. Jiang, P. Gao, L. Tian and X. J. Peng, *J. Am. Chem. Soc.*, 2014, **136**, 9590–9597; (*b*) X. Xiong, L. Zheng, J. Yan, F. Ye, Y. Qian and F. Song, *RSC Adv.*, 2015, **5**, 53660–53664; (*c*) J. Zhang, R. Chen, Z. Zhu, C. Adachi, X. Zhang and C. Lee, *ACS Appl. Mater. Interfaces*, 2015, **7**, 26266–26274; (*d*) T. Li, D. Yang, L. Zhai, S. Wang, B. Zhao, N. Fu, L. Wang, Y. Tao and W. Huang, *Adv. Sci.*, 2017, **4**, 1600166; (*e*) Y. Wu, F. Song, W. Luo, Z. Liu, B. Song and X. Peng, *ChemPhotoChem*, 2017, **1**, 79–83; (*f*) S. Gan, J. Zhou, T. A. Smith, H. Su, W. Luo, Y. Hong, Z. Zhao and B. Z. Tang, *Mater. Chem. Front.*, 2017, **1**, 2554–2558; (*g*) J. Huang, H. Nie, J. Zeng, Z. Zhuang, S. Gan, Y. Cai, J. Guo, S. J. Su, Z. Zhao and B. Z. Tang, *Angew. Chem., Int. Ed.*, 2017, **56**, 12971–12976.

10 F. Ni, Z. Wu, Z. Zhu, T. Chen, K. Wu, C. Zhong, K. An, D. Wei, D. Ma and C. Yang, *J. Mater. Chem. C*, 2017, **5**, 1363–1368.

11 H. Hofmeiera and U. S. Schubert, *Chem. Soc. Rev.*, 2004, **33**, 373–399.

12 K. A. Conners, *Binding constants, the measurement of molecular complex stability*, John Wiley and Sons, New York, 1987, vol. 25, pp. 565–566.

13 J. E. Coleman, *Annu. Rev. Biochem.*, 1992, **61**, 897–946.

14 S. Iuchi, *Cell. Mol. Life Sci.*, 2001, **58**, 625–635.

15 K. Zhang, Q. Yu, H. Wei, S. Liu, Q. Zhao and W. Huang, *Chem. Rev.*, 2018, **118**, 1770–1839.